

Ferroelectric HfO₂-ZrO₂ multilayers with reduced wake-up

Barnik Mandal^{*1,3}, Adrian-Marie Philippe², Nathalie Valle², Emmanuel Defay^{1,3},
Torsten Granzow¹, and Sebastjan Glinsek¹.

¹Smart Materials Unit, Luxembourg Institute of Science and Technology (LIST),
41 Rue de Brill, L-4422 Belvaux, Luxembourg.

²Advanced Analyses and Support Unit, Luxembourg Institute of Science and Technology (LIST),
41 Rue de Brill, L-4422 Belvaux, Luxembourg.

³University of Luxembourg, 2 Av. de l'Universite L,
L-4365, Esch-sur-Alzette, Luxembourg.

April 1, 2025

Corresponding author

Barnik Mandal (barnik.mandal@list.lu)

Keywords

multilayer hafnia zirconia; ferroelectric hafnia zirconia; multilayer thin films;

Abstract

Since the discovery of ferroelectricity in HfO_2 thin films, significant research has focused on Zr-doped HfO_2 and solid solution $(\text{Hf,Zr})\text{O}_2$ thin films. Functional properties can be further tuned via multilayering, however, this approach has not yet been fully explored in HfO_2 - ZrO_2 films. This work demonstrates ferroelectricity in a 50 nm thick, solution-processed HfO_2 - ZrO_2 multilayer film, marking it as the thickest multilayer film to date exhibiting ferroelectric properties. The multilayer structure was confirmed through transmission electron microscopy (TEM) and energy dispersive x-ray spectroscopy, with high-resolution TEM revealing grain continuity across multiple layers. This finding indicates that a polar phase in the originally paraelectric ZrO_2 layer, can be stabilized by the HfO_2 layer. The film attains a remanent polarization of $9 \mu\text{C}/\text{cm}^2$ and exhibits accelerated wake-up behavior, attributed to its higher breakdown strength resulting from the incorporation of multiple interfaces. These results offer a faster wake-up mechanism for thick ferroelectric hafnia films.

1 Introduction

The discovery of ferroelectricity in doped HfO_2 has garnered interest due to its compatibility with complementary metal-oxide-semiconductor (CMOS) technology.[1] Given the similar chemical and physical properties of HfO_2 and ZrO_2 , studies on ferroelectricity in ZrO_2 have also been conducted.[2] Both of these simple oxides are regarded as promising lead-free alternatives for non-volatile memory and piezoelectric applications. In 2016, Fan et al. demonstrated the stabilization of the ferroelectric orthorhombic phase in a ZrO_2 thin film produced by radio frequency magnetron sputtering, utilizing substrate-induced strain to promote transition from the paraelectric tetragonal phase (t-phase) to the ferroelectric orthorhombic phase (o-phase).[3] Starschich et al. reported thicker ZrO_2 and Hf-doped ZrO_2 ferroelectric films of 100 nm and 390 nm, respectively, using chemical solution deposition (CSD) with organometallic precursors.[2] The evolution of ferroelectricity in solid solutions of HfO_2 and ZrO_2 ($\text{Hf}_x\text{Zr}_{1-x}\text{O}_2$) has been intensively studied using various growth techniques, with reported properties ranging from ferroelectric- to antiferroelectric-like. The maximum remanent polarization P_r is observed typically around the composition $\text{Hf}_{0.5}\text{Zr}_{0.5}\text{O}_2$, while existence of a CMOS-compatible morphotropic phase boundary has been postulated for the composition $\text{Hf}_{0.3}\text{Zr}_{0.7}\text{O}_2$. [4–6]

Several experimental investigations reported ferroic HfO_2 - ZrO_2 multilayers.[7–11] The main drive behind the majority of these studies has been the stabilization of the ferroelectric phase and enhancement of properties in sub-20 nm multilayer films through mechanical confinement of the layers[7], increased interface energy[8] and lattice distortion caused by grain coalescence during thermal annealing.[9] Using Density Functional Theory, Dutta et al. demonstrated that small-size dopants like Si tend to form distinct layers in the orthorhombic ferroelectric polymorph, avoiding intermixing with Hf. Layering stabilizes the polar phase over non-polar polymorphs, strongly suggesting the use of multilayer structures instead of solid solutions.[12] Furthermore, Cheema et al. reported permittivity enhancement in ultrathin HfO_2 - ZrO_2 superlattices with mixed ferroelectric–antiferroelectric order, i.e., an effect not possible in conventional ferroelectrics.[11] These results demonstrate the potential advantages of multilayers in polar fluorite oxides.

In this work, we examine the stabilization of ferroelectricity and the wake-up be-

haviour in 50 nm multilayer La:HfO₂-ZrO₂ thin films, representing the thickest multilayer thin films studied to date. While there have been studies on thick Hf_{0.5}Zr_{0.5}O₂ solid-solution films,[2, 13] they have not specifically focused on multilayer structures. We prepared pure ZrO₂, La:HfO₂, and multilayer La:HfO₂-ZrO₂ films using a CSD process described in our previous publication.[14] La doping for HfO₂ layer was chosen based on density functional theory predictions, which suggested that La's larger ionic radius and lower electronegativity promote stabilization of the ferroelectric orthorhombic Pca2₁ phase.[15, 16] Experimental findings further validated the predictions, demonstrating a wide doping range and reduced polarization relaxation.[17] For clarity in the following discussion, the thin-film samples of La:HfO₂, ZrO₂, and La:HfO₂-ZrO₂ multilayers are referred to as HO, ZO, and HZO, respectively. It is observed that although the pure ZrO₂ film is paraelectric, the combination with the polar HfO₂ layer induces ferroelectricity in ZrO₂ layer of the HZO film. High-resolution transmission electron microscopy (HR-TEM) confirms that the polar phase extends through multiple layers. The HZO film exhibits ferroelectric properties with a remanent polarization (P_r) of 9 $\mu\text{C}/\text{cm}^2$, which is minor improvement to the conventional HO films. We further show that the multilayered HZO films can sustain higher electric fields than the HO film alone, resulting in significant reduction of wake-up cycles. The number of cycles required for polarization saturation in HZO decreased tenfold (from 10,000 to 1,000) compared to standard HO films.

2 Methods

Solution Preparation: Two 0.25 M precursor solutions were prepared, one containing La:HfO₂ for the HO film and the other containing ZrO₂ for the ZO film. Additionally, two solutions of La:HfO₂ and ZrO₂ with a concentration of 0.08 M were prepared for the multilayer HZO film. For 5% La-doped HfO₂, Hf(IV)-acetylacetonate (Alfa Aesar, 97%) and La(III)-acetate hydrate (Sigma-Aldrich, 99.9%) were used as metal precursors, with the La(III)-acetate hydrate being freeze-dried for 16 hours to remove crystal water. For pure ZrO₂, Zr(IV)-acetylacetonate (Sigma-Aldrich, 97%) was used. The powders were dissolved in propionic acid (Sigma-Aldrich, 99.5% purity) and then refluxed for 3 hours at 150 °C with magnetic stirring in an Ar atmosphere using a modified Schlenk apparatus.

Film Preparation: The solutions were spin-coated onto platinized Si substrates (Pt-Si, SINTEF) at 3000 rpm for 30 seconds. The platinum layer was strongly oriented in the (111) direction. After each spin-coating, a drying step was performed on a hot plate at 215 °C for 5 minutes. For the ZO and HO films, three 15 nm-thick amorphous layers were spin-coated from 0.25 M ZrO₂ and 0.25 M La:HfO₂ solutions, respectively. For the HZO sample, ten 5 nm-thick layers of La:HfO₂ and ZrO₂ were alternately deposited using 0.08 M La:HfO₂ and 0.08 M ZrO₂ solutions (see Figure 1(a)). The films were subsequently subjected to rapid thermal annealing (RTA) using an AS-Master 2000 (Annealsys) tool. In the RTA process, the chamber underwent a purging sequence by pumping down to a pressure below 4 mbar. Subsequently, the chamber was restored to atmospheric pressure while being filled with N₂ and O₂. N₂ and O₂ were pumped at flow rates of 1000 sccm each to establish an atmosphere with a 1:1 ratio. Following the chamber filling, the final crystallization step was initiated by reducing gas flow rates to 150 sccm:150 sccm for N₂:O₂. Films were then crystallized at 800 °C for 90 s with 50 °C s⁻¹ ramping rate. Circular top electrodes were evaporated on the film, each measuring 100 μm in diameter. These electrodes comprised two layers: first a 5 nm thick Ti adhesion layer, followed by a 100 nm thick Pt layer. The deposition was carried out using a Plassys evaporator under a pressure of 5x10⁻⁸ mbar. The electrodes were patterned by standard lithography and lift-off processes.

Characterization: A Bruker D8 Discover X-ray diffractometer with Cu K α radiation ($\lambda = 0.154$ nm) was used for grazing incidence (GI) and θ -2 θ X-ray diffraction (XRD). An incidence angle of 0.5° was used for GIXRD. The reference patterns for monoclinic, orthorhombic, and tetragonal HfO₂ were taken from the powder diffraction files with the numbers 00-034-0104, 04-005-5597, and 04-003-2612, respectively.[18] These same references were also applied to ZrO₂, as they have very similar crystalline structures.

Ferroelectric measurements were performed using a TF Analyzer 2000 (aixACCT, Germany). Polarization versus electric field loops were acquired using a 3 kHz bipolar triangular signal, following the application of a desired number of rectangular wake-up cycles at 3 kHz. Two distinct sets of wake-up cycles were conducted on the HZO and HO films. The first set, referred to as procedure 1, consisted of a 1000-cycle wake-up at

15 V. The second set, procedure 2, involved 7000 cycles, performed as seven consecutive 1000-cycle wake-ups, with increasing voltages from 8 V to 15 V.

The (Scanning) Transmission Electron Microscopy ((S)TEM) analyses were performed on a JEOL JEM-F200 cold FEG microscope operating at an acceleration voltage of 200 kV. TEM lamella was prepared following the “lift-out” method with a FEI Helios Nanolab 650 Focussed Ion Beam Scanning Electron Microscope (FIB-SEM). X-ray Energy Dispersive Spectroscopy (EDS), using dual JEOL 100 mm² Silicon Drift Detectors, was performed in STEM mode allowing elemental maps analysis. High Resolution TEM (HRTEM) imaging combined with Fast Fourier Transform (FFT) computation was performed to identify crystalline phases observed throughout the thin film. The reference patterns for monoclinic, orthorhombic, and tetragonal HfO₂ were taken from the powder diffraction files with the numbers 04-002-2772, 04-005-5597, and 04-027-1007, respectively.[18]

3 Results and discussion

Figure 1(a) presents a structural schematic of the multilayer HZO film, which consists of ten 5 nm-thick layers of alternately deposited La:HfO₂ and ZrO₂, starting with La:HfO₂ and ending with ZrO₂. The bright-field STEM image in Figure 1(b) reveals the expected multilayered stack, indicated by the contrast variation between the La:HfO₂ and ZrO₂ layers, with two Pt-based electrodes enclosing the stack. EDS spectrum (see Supporting Information) to generate the line profile in Figure 1(c) was extracted from the area outlined by the white box in Figure 1(b). The oscillating behavior of the Hf M and Zr K EDS line profiles in Figure 1(c), along with EDS cross-section mapping (see Supporting Information) further validates the multilayered structure of the film, with the Ti K line indicating where the film terminates. The grazing incident X-ray diffraction (GIXRD) patterns of the HO, ZO, and HZO films are illustrated in Figure 1(d). The patterns show the characteristic features typically observed in HfO₂ and ZrO₂ thin films, i.e., a pronounced peak at 30.6 ° and a weaker peak at 35.5 °, indicative of the orthorhombic polar planes (111) and (002), respectively. However, note that the structural similarities between the polar orthorhombic and non-polar tetragonal phases lead to significant

overlap of their reflections, making it challenging to distinguish them in laboratory XRD experiment. Additionally, a broad shoulder peak between $\sim 31^\circ$ and 31.5° is also present, which may correspond to a monoclinic phase ($P2_1/c$).

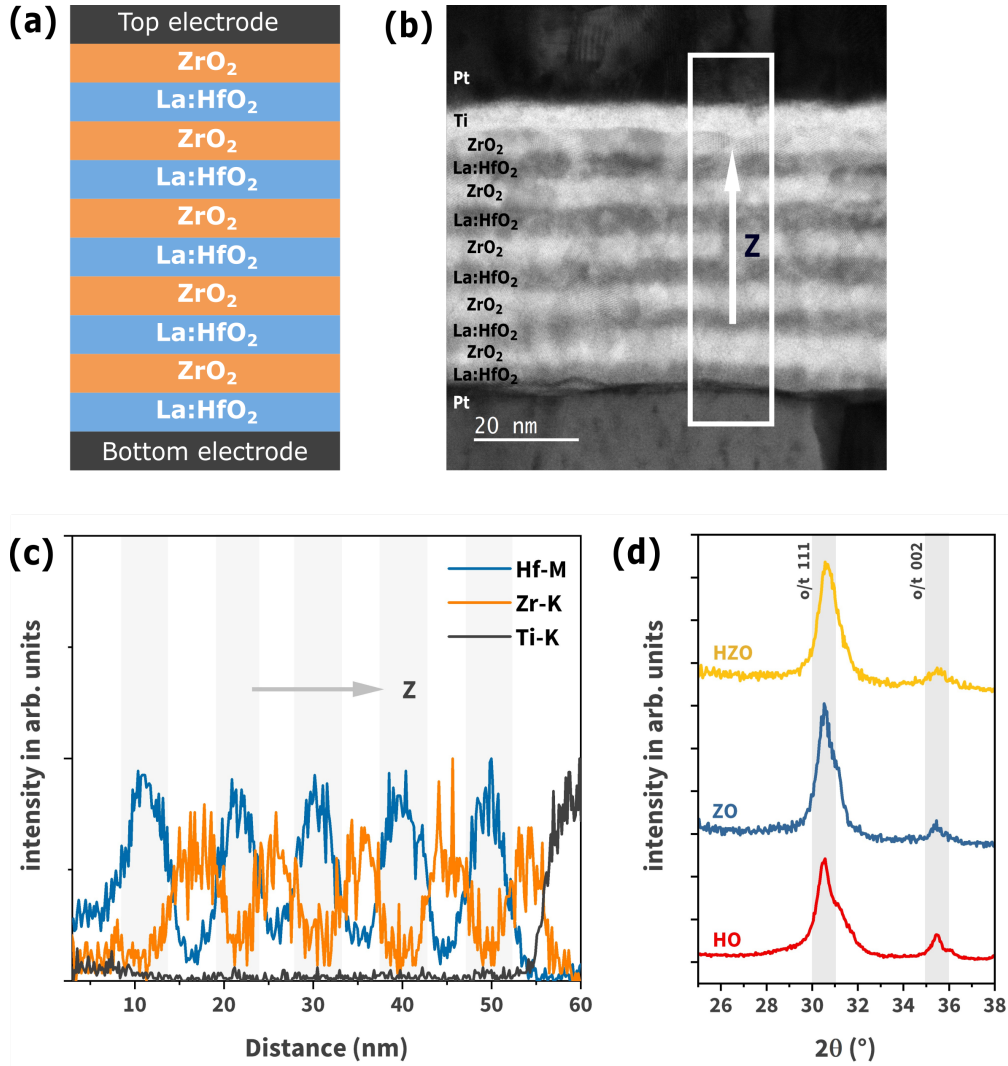


Figure 1: (a) Structural schematics, (b) bright-field STEM image of HZO multilayer film with Pt/Ti top electrode and Pt bottom electrode, (c) STEM-EDS line profile of the HZO multilayer. Z is the direction of growth. (d) GIXRD patterns of the HO film, ZO film and HZO multilayer film. The main peaks are labeled with o/t (orthorhombic/tetragonal), which correspond to the reference patterns of $Pca2_1$ and $P4_2/nmc$ phases, respectively.[18]

The current density-electric field and polarization-electric field hysteresis loops after wake-up cycling are shown in Figure 2. The ZO film does not show any switching current and is therefore paraelectric. The HO and multilayered HZO films exhibit prominent switching current peaks. The HO film has a positive remanent polarization (P_r) of $8 \mu\text{C}/\text{cm}^2$, with coercive field (E_c) of 1.5 MV cm^{-1} . HZO has a positive P_r of $9 \mu\text{C}/\text{cm}^2$, with E_c of 1.2 MV cm^{-1} . If the ZrO_2 layers were purely dielectric, they would have acted as dead layers, reducing the effective electric field across the film. This, in turn, would result in a decrease in remanent polarization and an increase in the coercive field[19], which is not observed in this case. Therefore, it can be concluded that HZO and HO samples have effective ferroelectric layers of almost identical thicknesses. Interesting to note is that when multilayers are prepared with ZrO_2 as the initial layer, poor ferroelectric properties are observed in the multilayer (see Supporting Information). This is likely due to the non-polar phase of the initial ZrO_2 layer. We can speculate that this could be improved if the polar phase would be stabilized in this first layer by optimizing the processing parameters. Similar result is reported by van Gent et al.[20] in epitaxial rhombohedral $\text{Hf}_{1-x}\text{Zr}_x\text{-ZrO}_2$ superlattices prepared via pulsed laser deposition, indicating that this effect is intrinsic to $\text{HfO}_2\text{-ZrO}_2$ multilayers, regardless of the fabrication method, type of ferroelectric phase or microstructure.

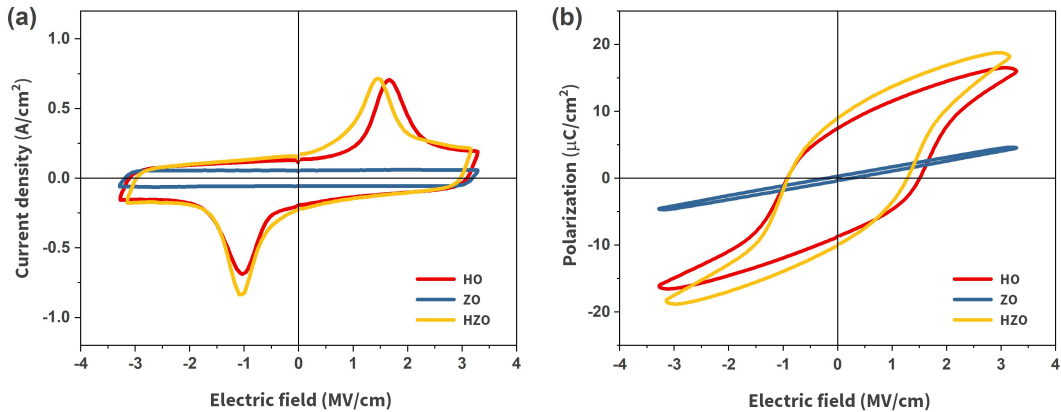


Figure 2: (a) Current density versus electric field loops, and (b) polarization versus electric field loops of the three films.

To gain a better understanding of the phase and grain orientation, cross-sectional high-resolution transmission electron microscopy (HRTEM) was performed on the HZO sample and the result is shown in Figure 3(a). Lattice fringes extending across multiple layers are observed, suggesting a continuation of grains and their orientation through the layers with different composition. The Fast Fourier Transform (FFT) of an exemplary area is presented in Figure 3(b). The FFT experimental pattern was compared with the simulated diffraction patterns from PDF cards of monoclinic (space group $P2_1/c$), orthorhombic (space group $Pca2_1$) and tetragonal phase (space group $P4_2/nmc$). It aligns well with the simulated diffraction pattern of the ferroelectric o-phase along the $[-101]$ zone axis (Figure 3(c)) and non-polar t-phase along the $[-111]$ zone axis (Figure 3(d)). The ratio of the distances from the center to spots 1 and 2, and ratio from the center to spots 2 and 3 in the experimental FFT, are 1.62 and 0.86, respectively. These values are closely aligned with those obtained from simulated patterns of the o-phase and t-phase (see Supporting Information). The observed ferroelectric switching in the electrical measurements suggests the presence of the o-phase rather than the t-phase in the presented lattice fringe. However, the possibility of the diffractogram corresponding to the m-phase can be ruled out (see Supporting Information).

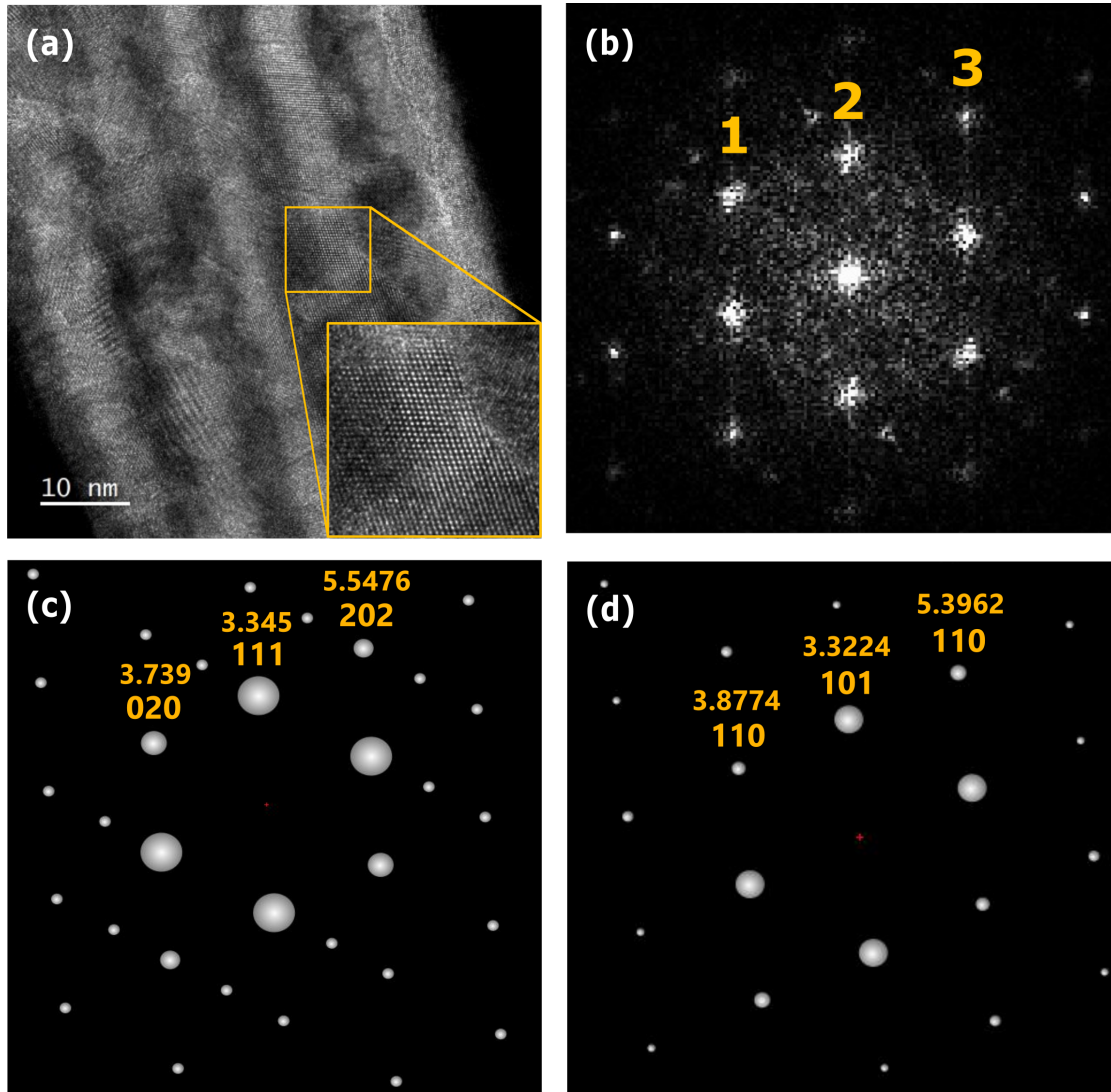


Figure 3: (a) Cross-sectional HRTEM images of field cycled HZO multilayer film. (b) FFT diffraction pattern of the squared area. Simulated diffraction pattern of (c) orthorhombic HfO₂ along [-101] zone axis (space group Pca2₁) and (d) tetragonal HfO₂ along [-111] zone axis (space group P4₂/nmc), .

While the conventional HO and multilayer HZO films show comparable ferroelectric properties, an important difference was observed during the wake-up cycling. Figure 4(a) illustrates the increase of remanent polarization $2P_r$ with respect to the number of wake-up cycles. Two distinct sets of wake-up cycles were conducted on the HZO and HO films. The first set, referred to as procedure 1, consisted of a 1000-cycle wake-up at an electric field of approximately 3 MV cm^{-1} , exceeding the coercive field of typical HfO_2 films. The second set, procedure 2, involved 7000 cycles, performed as seven consecutive 1000-cycle wake-ups, with the electric field gradually increasing from about 0.8 MV cm^{-1} to around 3 MV cm^{-1} . The HO film could not withstand the immediate application of fields exceeding E_c and typically broke down after approximately 10 cycles, making wake-up cycling using procedure 1 impossible. HZO film, on the other hand, revealed an escalated wake-up behaviour upon treating with procedure 1. The pristine loops of HZO (from procedure 1) and HO (from procedure 2) films are presented in 4(b), where HZO shows a propeller-shaped hysteresis loop with non-zero remanent polarization, very similar to $\text{Hf}_x\text{Zr}_{1-x}\text{O}_2$ films reported in previous studies.[5, 7] Experimental observations and theoretical modeling have linked that to an electric field-induced phase transition from the tetragonal (T) phase to the orthorhombic o-III phase.[2, 21] Furthermore, studies have shown that propeller-shaped hysteresis loops arise due to defect pinning and are also influenced by the evolution of charged domain walls.[22, 23] Figure 4(c) presents the hysteresis loops after 1000 cycles, showing that HZO reached a maximum $2P_r$ of $18 \mu\text{C/cm}^2$. In comparison, the HO film required 7000 cycles to achieve comparable $2P_r$ (see Figure 4(d)). When using procedure 2, HZO showed nearly identical wake-up behavior to the HO sample (see Figure 4(a)).

Wake-up field cycling is typically performed in hafnia-based ferroelectrics to improve ferroelectric response through redistribution of defects, typically oxygen vacancies.[24, 25] However, these defects, often located at grain boundaries, interfaces or domain walls, can also form conductive filaments upon exposure to electric field.[26–28] Performing wake-up cycles directly at or above the coercive field is therefore detrimental to dielectric properties of conventional HO films. We hypothesize that the reason multilayer HZO films can endure direct application of high fields are multiple $\text{La:HfO}_2\text{-ZrO}_2$ interfaces, which disrupt the formation of conductive filaments along the film thickness. Breakdown measurements were performed on both samples (see Supporting Information), and early

breakdown was indeed observed in the HO film. Furthermore, endurance improved from 10^4 cycles in HO films to 10^5 cycles in HZO films (see Supporting Information). Note that enhanced cycling endurance from 10^6 to 10^9 cycles is observed in epitaxial rhombohedral $\text{Hf}_{1-x}\text{Zr}_x\text{-ZrO}_2$ superlattices, confirming that multilayering is an effective approach to robust ferroelectric hafnia-based films.[20] Beyond hafnia, Sun et al.[29] achieved a breakdown strength of 4.5 MV cm^{-1} in BZT-BCT multilayer films, compared to 1 MV cm^{-1} in single-layer BZT and BCT films of the same thickness. They explained the effect by inhibited propagation and growth of "electric trees" in the films with engineered interfaces. In addition to multilayering, early fatigue in ferroelectric thin films has been reported to be tackled through strategies such as engineering of oxygen vacancies, suppressing defect diffusion, and introducing compositional inhomogeneity. [30–32]

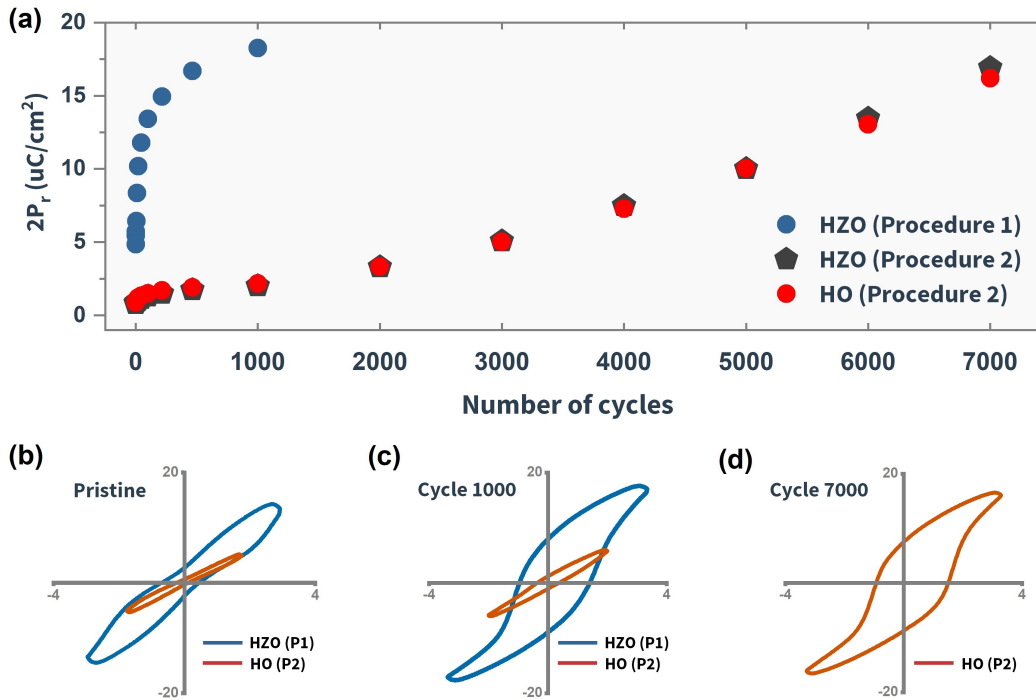


Figure 4: (a) Remanent polarization $2P_r$ vs. number of wake-up cycles for HZO and HO films. (b) Pristine loops of HZO and HO, acquired from procedure 1 and procedure 2, respectively. (c) HZO and HO loops measured after 1000 cycles following procedure 1 and procedure 2, respectively. (d) HO loop measured after 7000 cycles following procedure 2, for the HZO film, maximum $2P_r$ was achieved by procedure 1 (1000 cycles), therefore no loop is recorded after 7000 cycles. [P1: Procedure 1, P2: Procedure 2]

4 Conclusion and outlook

In summary, we demonstrated ferroelectricity in solution-processed 50 nm-thick HZO multilayer film. The ferroelectric properties of the multilayer thin film were investigated through the characterization of compositional profiles, crystalline phases, and electrical measurements. Although the pure ZrO_2 films processed were paraelectric in nature, the synthesis of a multilayer structure with HfO_2 induced a polar phase in ZrO_2 through the La-doped HfO_2 layer. The HZO film exhibits ferroelectric properties, with a remanent polarization of $9 \mu\text{C cm}^{-2}$ and a coercive field of 1.2 MV cm^{-1} . Additionally, as prepared HZO films can endure higher electric fields due to the presence of multiple interfaces, which significantly reduces the wake-up cycles - an improvement by an order of magnitude compared to the conventional films. This study highlights a novel pathway to enhance the wake-up properties of ferroelectric HfO_2 and ZrO_2 -based thin films by introducing interfaces, rather than relying solely on solid solutions. This approach can be extended to the growth of thicker multilayer films for piezoelectric applications, as the improved wake-up properties and reduced early breakdown during extended cycling help address the challenges typically associated with thicker films.

Acknowledgments

BM, TG and SG acknowledge Luxembourg National Research Fund (FNR) for supporting this work through the project TRICOLOR (INTER/NWO/20/15079143/TRICOLOR). The authors would like to thank Prof. Beatriz Noheda and Johanna van Gent for valuable discussions on the results.

Supporting Information

The Supporting Information is available free of charge on the ACS Publications website and from the author. Polarization hysteresis of ZHO film, EDS and FFT diffractogram of HZO film, leakage and fatigue measurements of HO and HZO films.

Declaration of Interest

The authors declare no competing interests.

Data Availability statement

The raw data generated in this study have been deposited in the Zenodo repository under <https://doi.org/10.5281/zenodo.14893377>.

References

- [1] T. S. Böске, J. Müller, D. Bräuhaus, U. Schröder, and U. Böttger. “Ferroelectricity in hafnium oxide thin films”. In: *Applied Physics Letters* 99.10 (Sept. 2011), p. 102903. ISSN: 0003-6951. DOI: 10.1063/1.3634052.
- [2] S. Starschich, T. Schenk, U. Schroeder, and U. Boettger. “Ferroelectric and piezoelectric properties of $\text{Hf}_{1-x}\text{Zr}_x\text{O}_2$ and pure ZrO_2 films”. In: *Applied Physics Letters* 110.18 (May 2017), p. 182905. ISSN: 0003-6951. DOI: 10.1063/1.4983031.
- [3] Zhen Fan, Jinyu Deng, Jingxian Wang, Ziyang Liu, Ping Yang, Juanxiu Xiao, Xiaobing Yan, Zhili Dong, John Wang, and Jingsheng Chen. “Ferroelectricity emerging in strained (111)-textured ZrO_2 thin films”. In: *Applied Physics Letters* 108.1 (Jan. 2016). ISSN: 1077-3118. DOI: 10.1063/1.4939660. URL: <http://dx.doi.org/10.1063/1.4939660>.
- [4] Shuhei Nakayama, Hiroshi Funakubo, and Hiroshi Uchida. “Crystallization behavior and ferroelectric property of $\text{HfO}_2\text{-ZrO}_2$ films fabricated by chemical solution deposition”. In: *Japanese Journal of Applied Physics* 57.11S (Sept. 2018), 11UF06. ISSN: 1347-4065. DOI: 10.7567/jjap.57.11uf06. URL: <http://dx.doi.org/10.7567/JJAP.57.11UF06>.
- [5] Johannes Müller, Tim S. Böске, Uwe Schröder, Stefan Mueller, Dennis Bräuhaus, Ulrich Böttger, Lothar Frey, and Thomas Mikolajick. “Ferroelectricity in Simple Binary ZrO_2 and HfO_2 ”. In: *Nano Letters* 12.8 (Aug. 2012), pp. 4318–4323. ISSN: 1530-6984. DOI: 10.1021/nl302049k. URL: <https://doi.org/10.1021/nl302049k>.
- [6] Kai Ni, Atanu Saha, Wriddhi Chakraborty, Huacheng Ye, Benjamin Grisafe, Jeffrey Smith, G. Bruce Rayner, Sumeet Gupta, and Suman Datta. “Equivalent Oxide Thickness (EOT) Scaling With Hafnium Zirconium Oxide High-K Dielectric Near Morphotropic Phase Boundary”. In: *2019 IEEE International Electron Devices Meeting (IEDM)*. IEEE, Dec. 2019. DOI: 10.1109/iedm19573.2019.8993495. URL: <http://dx.doi.org/10.1109/IEDM19573.2019.8993495>.
- [7] Y.W. Lu, J. Shieh, and F.Y. Tsai. “Induction of ferroelectricity in nanoscale $\text{ZrO}_2/\text{HfO}_2$ bilayer thin films on Pt/Ti/SiO₂/Si substrates”. In: *Acta Materialia* 115 (Aug. 2016), 68–75. ISSN: 1359-6454. DOI: 10.1016/j.actamat.2016.05.029. URL: <http://dx.doi.org/10.1016/j.actamat.2016.05.029>.
- [8] Haiyan Chen, Lin Tang, Hang Luo, Xi Yuan, and Dou Zhang. “Modulation of ferroelectricity in atomic layer deposited $\text{HfO}_2/\text{ZrO}_2$ multilayer films”. In: *Materials Letters* 313 (Apr. 2022), p. 131732. ISSN: 0167-577X. DOI: 10.1016/j.matlet.2022.131732. URL: <http://dx.doi.org/10.1016/j.matlet.2022.131732>.
- [9] Stephen L. Weeks, Ashish Pal, Vijay K. Narasimhan, Karl A. Littau, and Tony Chiang. “Engineering of Ferroelectric $\text{HfO}_2\text{-ZrO}_2$ Nanolaminates”. In: *ACS Applied Materials Interfaces* 9.15 (Apr. 2017), 13440–13447. ISSN: 1944-8252. DOI: 10.1021/acsami.7b00776. URL: <http://dx.doi.org/10.1021/acsami.7b00776>.

- [10] Min Hyuk Park, Han Joon Kim, Gwangyeop Lee, Jaehong Park, Young Hwan Lee, Yu Jin Kim, Taehwan Moon, Keum Do Kim, Seung Dam Hyun, Hyun Woo Park, Hye Jung Chang, Jung-Hae Choi, and Cheol Seong Hwang. “A comprehensive study on the mechanism of ferroelectric phase formation in hafnia-zirconia nanolaminates and superlattices”. In: *Applied Physics Reviews* 6.4 (Nov. 2019). ISSN: 1931-9401. DOI: 10.1063/1.5118737. URL: <http://dx.doi.org/10.1063/1.5118737>.
- [11] Suraj S. Cheema, Nirmaan Shanker, Li-Chen Wang, Cheng-Hsiang Hsu, Shang-Lin Hsu, Yu-Hung Liao, Matthew San Jose, Jorge Gomez, Wriddhi Chakraborty, Wenshen Li, Jong-Ho Bae, Steve K. Volkman, Daewoong Kwon, Yoonsoo Rho, Gianni Pinelli, Ravi Rastogi, Dominick Pipitone, Corey Stull, Matthew Cook, Brian Tyrrell, Vladimir A. Stoica, Zhan Zhang, John W. Freeland, Christopher J. Tassone, Apurva Mehta, Ghazal Saheli, David Thompson, Dong Ik Suh, Won-Tae Koo, Kab-Jin Nam, Dong Jin Jung, Woo-Bin Song, Chung-Hsun Lin, Seunggeol Nam, Jinseong Heo, Narendra Parihar, Costas P. Grigoropoulos, Padraic Shafer, Patrick Fay, Ramamoorthy Ramesh, Souvik Mahapatra, Jim Ciston, Suman Datta, Mohamed Mohamed, Chenming Hu, and Sayeef Salahuddin. “Ultrathin ferroic HfO₂-ZrO₂ superlattice gate stack for advanced transistors”. In: *Nature* 604.7904 (Apr. 2022), 65–71. ISSN: 1476-4687. DOI: 10.1038/s41586-022-04425-6. URL: <http://dx.doi.org/10.1038/s41586-022-04425-6>.
- [12] Sangita Dutta, Hugo Aramberri, Tony Schenk, and Jorge Íñiguez. “Effect of Dopant Ordering on the Stability of Ferroelectric Hafnia”. In: *physica status solidi (RRL) – Rapid Research Letters* 14.6 (Mar. 2020). ISSN: 1862-6270. DOI: 10.1002/pssr.202000047. URL: <http://dx.doi.org/10.1002/pssr.202000047>.
- [13] Tony Schenk, Nicolas Godard, Aymen Mahjoub, Stephanie Girod, Aleksander Matavz, Vid Bobnar, Emmanuel Defay, and Sebastjan Glinsek. “Toward Thick Piezoelectric HfO₂ -Based Films”. In: *physica status solidi (RRL) – Rapid Research Letters* 14.3 (Dec. 2019), p. 1900626. DOI: 10.1002/pssr.201900626.
- [14] B. Mandal, N. Valle, B. E. Adib, S. Girod, K. Menguelti, Y. Fleming, P. Grysan, E. Defay, and S. Glinsek. “Control of Ferroelectricity in Solution-Processed Hafnia Films Through Annealing Atmosphere”. In: *Advanced Electronic Materials* 2024 (2024), p. 2300893. DOI: 10.1002/aelm.202300893. URL: <https://doi.org/10.1002/aelm.202300893>.
- [15] Rohit Batra, Tran Doan Huan, George A. Rossetti, and Rampi Ramprasad. “Dopants Promoting Ferroelectricity in Hafnia: Insights from a comprehensive Chemical Space Exploration”. In: *Chemistry of Materials* 29.21 (Oct. 2017), 9102–9109. ISSN: 1520-5002. DOI: 10.1021/acs.chemmater.7b02835. URL: <http://dx.doi.org/10.1021/acs.chemmater.7b02835>.
- [16] Robin Materlik, Christopher Künneth, Max Falkowski, Thomas Mikolajick, and Alfred Kersch. “Al-, Y-, and La-doping effects favoring intrinsic and field induced ferroelectricity in HfO₂: A first principles study”. In: *Journal of Applied Physics* 123.16 (Apr. 2018). ISSN: 1089-7550. DOI: 10.1063/1.5021746. URL: <http://dx.doi.org/10.1063/1.5021746>.

- [17] Uwe Schroeder, Claudia Richter, Min Hyuk Park, Tony Schenk, Milan Pešić, Michael Hoffmann, Franz P. G. Fengler, Darius Pohl, Bernd Rellinghaus, Chuanzhen Zhou, Ching-Chang Chung, Jacob L. Jones, and Thomas Mikolajick. “Lanthanum-Doped Hafnium Oxide: A Robust Ferroelectric Material”. In: *Inorganic Chemistry* 57.5 (Feb. 2018), 2752–2765. ISSN: 1520-510X. DOI: 10.1021/acs.inorgchem.7b03149. URL: <http://dx.doi.org/10.1021/acs.inorgchem.7b03149>.
- [18] *ICDD Database PDF4+ v4.23*. 2023.
- [19] Y.J. Zhang, X.J. Zheng, F. Jiao, and H.P. Hu. “The effect of strain and dead layer on the nonlinear electric-mechanical behavior of ferroelectric thin films”. In: *Computational Materials Science* 77 (Sept. 2013), 377–383. ISSN: 0927-0256. DOI: 10.1016/j.commatsci.2013.04.062. URL: <http://dx.doi.org/10.1016/j.commatsci.2013.04.062>.
- [20] J. van Gent, E. Kiens, and B. Noheda. “Highly polar and cyclable epitaxial $\text{Hf}_{1-x}\text{Zr}_x\text{O}_2\text{-ZrO}_2$ superlattices”. In: (2024). In preparation.
- [21] Sebastian E. Reyes-Lillo, Kevin F. Garrity, and Karin M. Rabe. “Antiferroelectricity in thin-film from first principles”. In: *Physical Review B* 90.14 (Oct. 2014). ISSN: 1550-235X. DOI: 10.1103/physrevb.90.140103. URL: <http://dx.doi.org/10.1103/PhysRevB.90.140103>.
- [22] Furqan Mehmood, Thomas Mikolajick, and Uwe Schroeder. “Wake-Up Mechanisms in Ferroelectric Lanthanum-Doped $\text{Hf}_{0.5}\text{Zr}_{0.5}\text{O}_2$ Thin Films”. In: *physica status solidi (a)* 217.22 (Sept. 2020). ISSN: 1862-6319. DOI: 10.1002/pssa.202000281. URL: <http://dx.doi.org/10.1002/pssa.202000281>.
- [23] Pingan Zhou, Binjian Zeng, Wanzhen Yang, Jiajia Liao, Fanqi Meng, Qinghua Zhang, Lin Gu, Shuaizhi Zheng, Min Liao, and Yichun Zhou. “Intrinsic 90° charged domain wall and its effects on ferroelectric properties”. In: *Acta Materialia* 232 (June 2022), p. 117920. ISSN: 1359-6454. DOI: 10.1016/j.actamat.2022.117920. URL: <http://dx.doi.org/10.1016/j.actamat.2022.117920>.
- [24] Milan Pešić, Franz Paul Gustav Fengler, Luca Larcher, Andrea Padovani, Tony Schenk, Everett D. Grimley, Xiahao Sang, James M. LeBeau, Stefan Slesazek, Uwe Schroeder, and Thomas Mikolajick. “Physical Mechanisms behind the Field-Cycling Behavior of HfO_2 -Based Ferroelectric Capacitors”. In: *Advanced Functional Materials* 26.25 (May 2016), 4601–4612. ISSN: 1616-3028. DOI: 10.1002/adfm.201600590. URL: <http://dx.doi.org/10.1002/adfm.201600590>.
- [25] Pengfei Jiang, Qing Luo, Xiaoxin Xu, Tiancheng Gong, Peng Yuan, Yuan Wang, Zhaomeng Gao, Wei Wei, Lu Tai, and Hangbing Lv. “Wake-Up Effect in HfO_2 -Based Ferroelectric Films”. In: *Advanced Electronic Materials* 7.1 (Nov. 2020). ISSN: 2199-160X. DOI: 10.1002/aelm.202000728. URL: <http://dx.doi.org/10.1002/aelm.202000728>.
- [26] Benjamin Max, Milan Pesic, Stefan Slesazek, and Thomas Mikolajick. “Interplay between ferroelectric and resistive switching in doped crystalline HfO_2 ”. In: *Journal of Applied Physics* 123.13 (Apr. 2018). ISSN: 1089-7550. DOI: 10.1063/1.5015985. URL: <http://dx.doi.org/10.1063/1.5015985>.

- [27] Zhongshan Xu, Xiaona Zhu, Guo-Dong Zhao, David Wei Zhang, and Shaofeng Yu. “Oxygen vacancies stabilized 180° charged domain walls in ferroelectric hafnium oxide”. In: *Applied Physics Letters* 124.1 (Jan. 2024). ISSN: 1077-3118. DOI: 10.1063/5.0179879. URL: <http://dx.doi.org/10.1063/5.0179879>.
- [28] Jaewook Lee, Kun Yang, Ju Young Kwon, Ji Eun Kim, Dong In Han, Dong Hyun Lee, Jung Ho Yoon, and Min Hyuk Park. “Role of oxygen vacancies in ferroelectric or resistive switching hafnium oxide”. In: *Nano Convergence* 10.1 (Dec. 2023). ISSN: 2196-5404. DOI: 10.1186/s40580-023-00403-4. URL: <http://dx.doi.org/10.1186/s40580-023-00403-4>.
- [29] Zixiong Sun, Chunrui Ma, Ming Liu, Jin Cui, Lu Lu, Jiangbo Lu, Xiaojie Lou, Lei Jin, Hong Wang, and Chun-Lin Jia. “Ultrahigh Energy Storage Performance of Lead-Free Oxide Multilayer Film Capacitors via Interface Engineering”. In: *Advanced Materials* 29.5 (Nov. 2016). ISSN: 1521-4095. DOI: 10.1002/adma.201604427. URL: <http://dx.doi.org/10.1002/adma.201604427>.
- [30] Keyu Bao, Jiajia Liao, Fei Yan, Shijie Jia, Binjian Zeng, Qiong Yang, Min Liao, and Yichun Zhou. “Enhanced Endurance and Imprint Properties in $\text{Hf}_{0.5}\text{Zr}_{0.5}\text{O}_2$ Ferroelectric Capacitors by Tailoring the Oxygen Vacancy”. In: *ACS Applied Electronic Materials* 5.8 (Aug. 2023), 4615–4623. ISSN: 2637-6113. DOI: 10.1021/acsaelm.3c00756. URL: <http://dx.doi.org/10.1021/acsaelm.3c00756>.
- [31] Mingshuang Kang, Yue Peng, Wenwu Xiao, Yueyuan Zhang, Zhe Wang, Peiyuan Du, Hao Jiang, Fenning Liu, Yan Liu, Yue Hao, and Genquan Han. “ HfO_2 - ZrO_2 Ferroelectric Capacitors with Superlattice Structure: Improving Fatigue Stability, Fatigue Recovery, and Switching Speed”. In: *ACS Applied Materials & Interfaces* 16.2 (Jan. 2024), 2954–2963. ISSN: 1944-8252. DOI: 10.1021/acsaemi.3c15732. URL: <http://dx.doi.org/10.1021/acsaemi.3c15732>.
- [32] Fei Yan, Ke Cao, Yang Chen, Jiajia Liao, Min Liao, and Yichun Zhou. “Optimization of ferroelectricity and endurance of hafnium zirconium oxide thin films by controlling element inhomogeneity”. In: *Journal of Advanced Ceramics* 13.7 (July 2024), 1023–1031. ISSN: 2227-8508. DOI: 10.26599/jac.2024.9220916. URL: <http://dx.doi.org/10.26599/JAC.2024.9220916>.

Supporting information: Ferroelectric HfO₂-ZrO₂ multilayers with reduced wake-up

Barnik Mandal^{*1,3}, Adrian-Marie Philippe², Nathalie Valle², Emmanuel Defay^{1,3},
Torsten Granzow¹, and Sebastjan Glinsek¹.

¹Smart Materials Unit, Luxembourg Institute of Science and Technology (LIST),
41 Rue de Brill, L-4422 Belvaux, Luxembourg.

²Advanced Analyses and Support Unit, Luxembourg Institute of Science and Technology (LIST),
41 Rue de Brill, L-4422 Belvaux, Luxembourg.

³University of Luxembourg, 2 Av. de l'Universite L,
L-4365, Esch-sur-Alzette, Luxembourg.

S1. ZHO film

Figure S1(a) presents a structural schematic of the multilayer ZHO film, which consists of ten 5 nm-thick layers of alternately deposited ZrO_2 and La:HfO_2 , starting with ZrO_2 and ending with La:HfO_2 . Figure S1(b) presents the electrical characterization of the ZHO film. After treatment with procedures 1 and 2, the ZHO film hardly shows switching current.

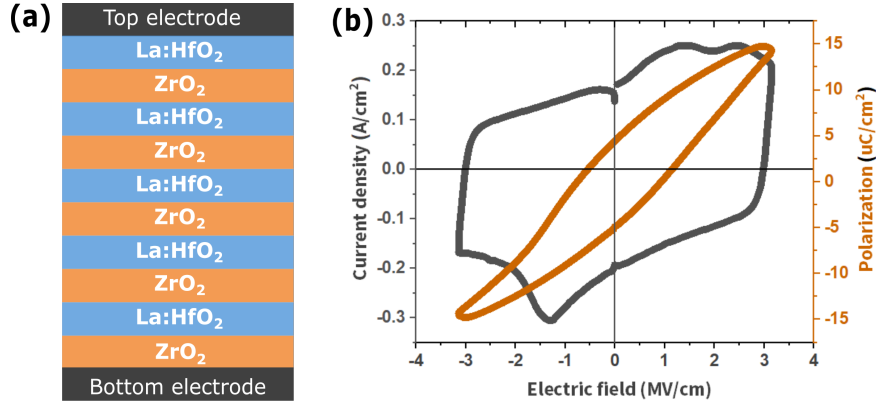


Fig. S1: (a) Structural schematics, and (b) hysteresis loops of the ZHO film after treating with procedure 2.

S2. Energy-dispersive X-ray spectroscopy (EDS)

The EDS spectrum in Figure S2 was utilized for line profile analysis. The EDS mapping of the cross-section profile of the HZO multilayer film is presented in Figure S3. Note that the green regions observed both at the top and at the bottom of the Hf map (S3 (b)) are an artifact due to the superimposition of the EDS Hf M and Pt M peaks. Similarly, the red regions visible both at the top and at the bottom of the Zr map (S3(c)) is an artifact due to the superimposition of EDS Zr K and Pt M peaks.

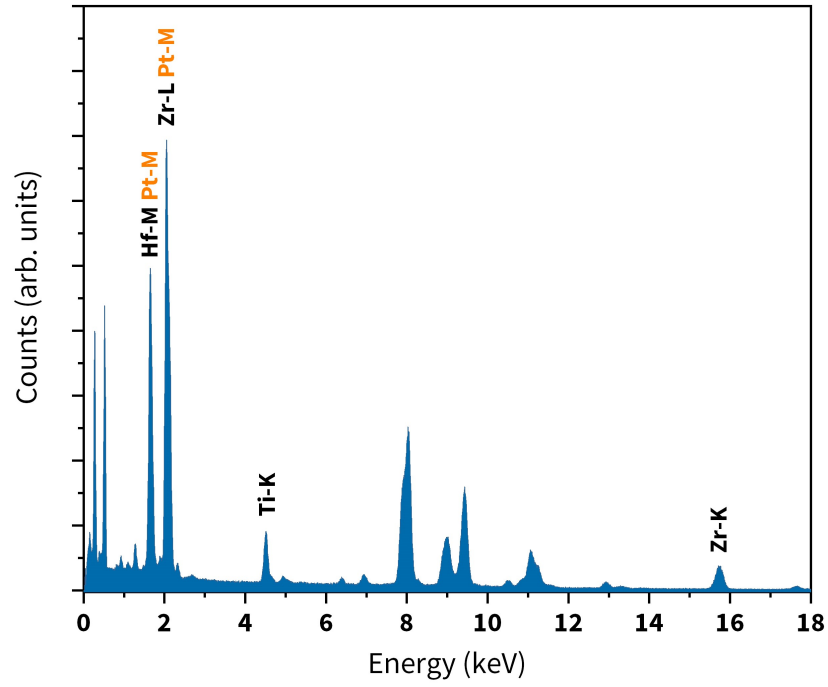


Fig. S2: EDS spectrum of HZO sample cross-section.

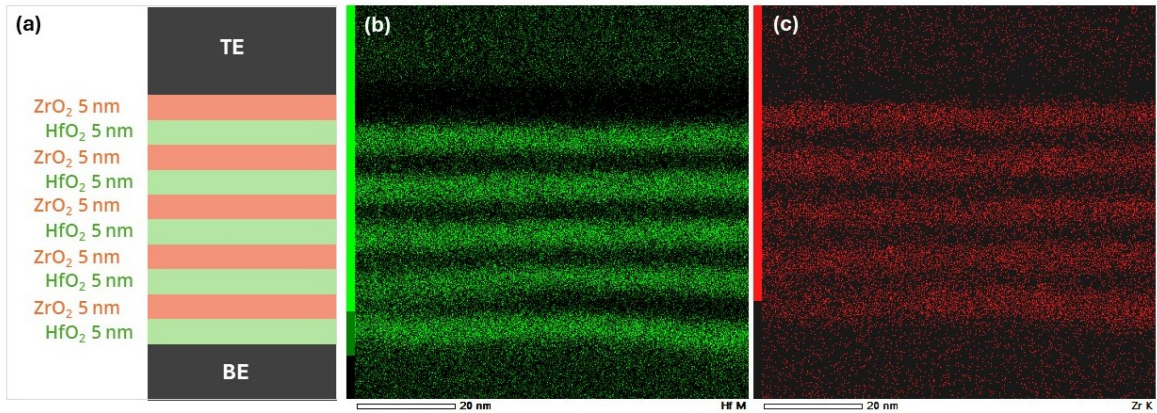


Fig. S3: (a) Multilayer schematic. EDS mapping of the cross-section profile of the HZO multilayer film consisting of (b) hafnia layers extracted from Hf-M and (c) zirconia layers extracted from Zr-K line profiles. TE: top electrode, BE: bottom electrode.

S3. Fast Fourier Transform (FFT)

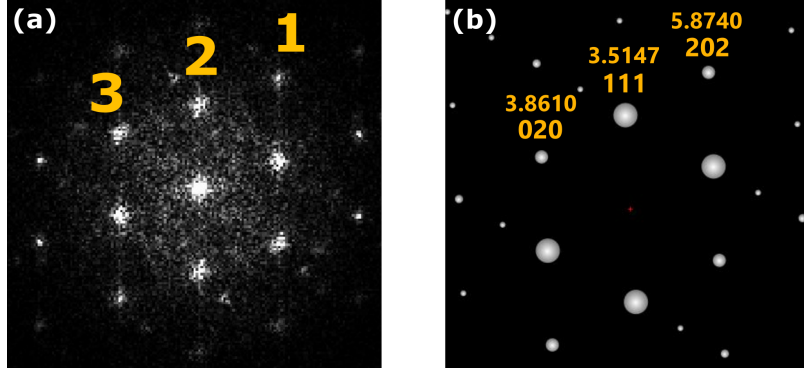


Fig. S4: (a) FFT diffractogram of the sample. (b) Simulated diffraction pattern of monoclinic HfO_2 along $[-101]$ zone axis (space group $P2_1c$).

Figure S4 shows the FFT diffractogram of the sample alongside simulated diffractograms for the m-phase. The bright central spot of the bi-dimensionnal FFT is a consequence of the smooth, i.e. long-range, transitions as well as the presence of noise in the original image Figure S4(a). Indeed, the center of the FFT is where the low frequency components of the real space are stored. All other bright spots visible on Figure S4(a) are related to higher frequencies corresponding to short-range periodicities on the original image and their respective spacing are measured from the center of the FFT image. A comparison of the spacings is provided in Table S1. The two-spot ratio of the sample is more closely aligned with the o-phase and t-phase than with the m-phase.

Table S1: Comparison of FFT spot spacing (in nm^{-1}) between the HZO sample data and the simulated phases shown in S4.

	HZO multilayer	o-phase	t-phase	m-phase
Spot 1	5.29	5.54	5.39	5.87
Spot 2	3.25	3.34	3.32	3.51
Spot 3	3.77	3.73	3.87	3.86
Ratio (spot 1/ spot 2)	1.62	1.65	1.62	1.67
Ratio (spot 2/ spot 3)	0.86	0.89	0.85	0.90

S4. Breakdown and fatigue measurements

Repeated measurements were performed on both the samples. Figure S5 presents the breakdown measurements for one example of each type. The HO films consistently broke down at ~ 2.3 MV/cm, while HZO sustained fields up to 4.0 MV/cm and beyond. Leakage current was below the measurement resolution for HO, while the HZO films showed an Ohmic behaviour with a resistivity ranging from $4 \cdot 10^7 \Omega\text{cm}$ to $7 \cdot 10^7 \Omega\text{cm}$.

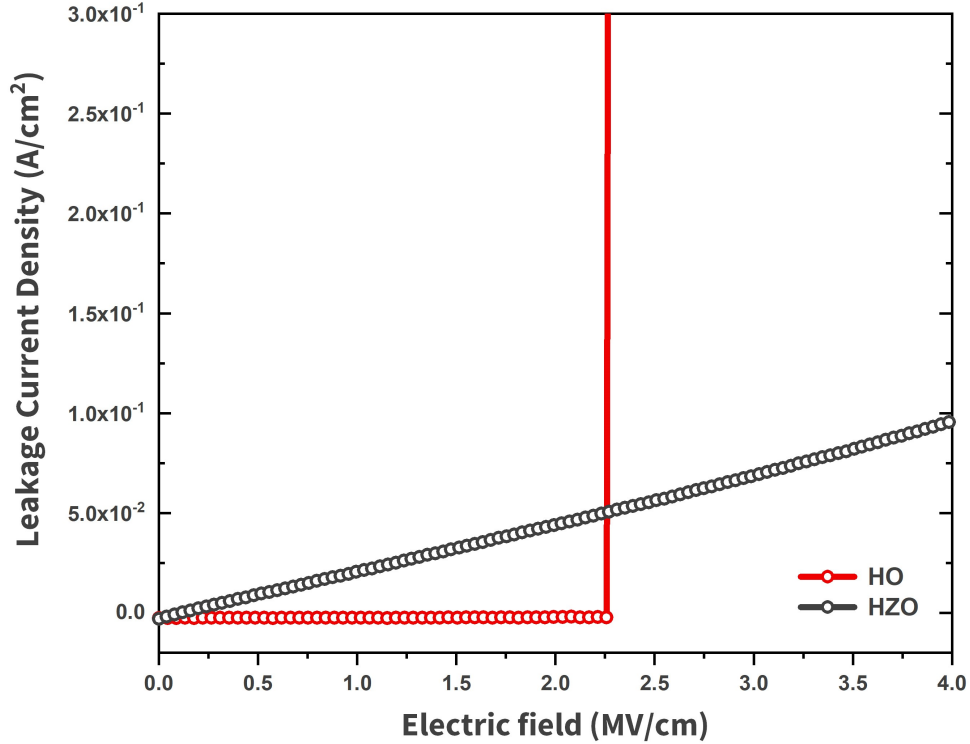


Fig. S5: Breakdown measurements of the pristine HO and HZO films. The measurement was performed on the TF Analyzer 2000 (aixACCT) tool with a step of 200 mV with a waiting time of 100 s for each data point.

Fatigue measurements are shown in Figure S6. The measurements were conducted at 3 kHz with gradually increasing the electric field from 0.8 MV cm^{-1} to 3 MV cm^{-1} (procedure 2). The HO sample experienced breakdown after 7,000 cycles, whereas the HZO multilayer films endured over 100,000 cycles, lasting an order of magnitude longer than the HO film. However, significant leakage current was observed after 50,000 cycles.

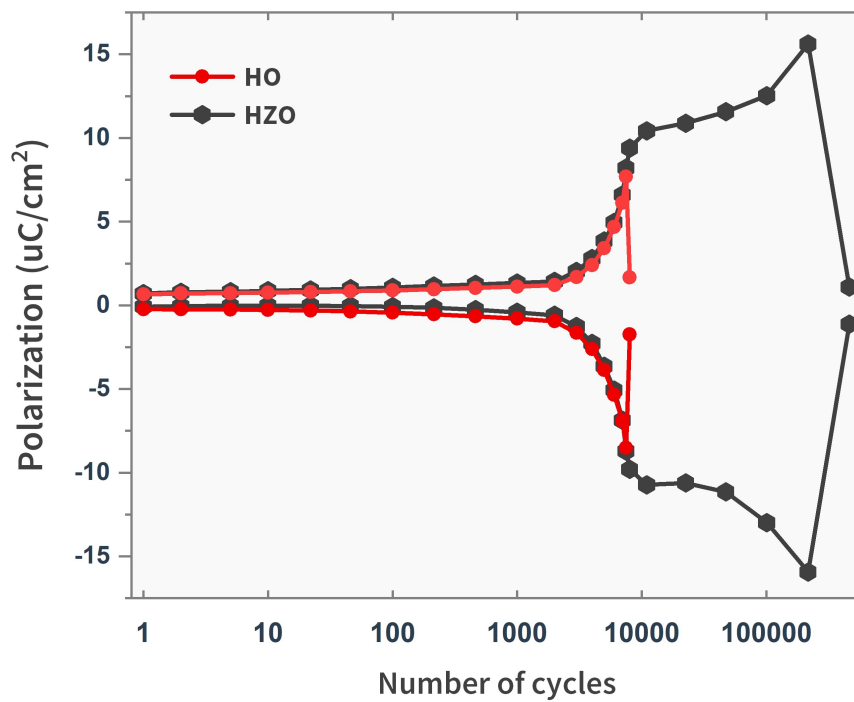


Fig. S6: Fatigue measurements. The measurements were conducted by cycling at 3 kHz with gradually increasing the electric field from 0.8 MV/cm to 3 MV/cm (procedure 2).